

# *Low-frequency contributions in the radiative efficiencies of HFC-236fa, HFC-245fa and HFC-43-10mee over the 225–298 K temperature range*

Article

Published Version

Creative Commons: Attribution-Noncommercial-No Derivative Works 4.0

Open Access

Alvarado-Jiménez, D., Tasinato, N. ORCID: <https://orcid.org/0000-0003-1755-7238>, Brownsword, R. ORCID: <https://orcid.org/0009-0005-5236-146X>, Weidmann, D. ORCID: <https://orcid.org/0000-0002-0178-7904>, Buizza, R. and Shine, K. P. ORCID: <https://orcid.org/0000-0003-2672-9978> (2026) Low-frequency contributions in the radiative efficiencies of HFC-236fa, HFC-245fa and HFC-43-10mee over the 225–298 K temperature range. *Journal of Quantitative Spectroscopy and Radiative Transfer*, 357. 109908. ISSN 1879-1352 doi: 10.1016/j.jqsrt.2026.109908 Available at <https://centaur.reading.ac.uk/128931/>

It is advisable to refer to the publisher's version if you intend to cite from the work. See [Guidance on citing](#).

To link to this article DOI: <http://dx.doi.org/10.1016/j.jqsrt.2026.109908>

Publisher: Elsevier

All outputs in CentAUR are protected by Intellectual Property Rights law, including copyright law. Copyright and IPR is retained by the creators or other copyright holders. Terms and conditions for use of this material are defined in the [End User Agreement](#).

[www.reading.ac.uk/centaur](http://www.reading.ac.uk/centaur)

## **CentAUR**

Central Archive at the University of Reading

Reading's research outputs online



Contents lists available at ScienceDirect

## Journal of Quantitative Spectroscopy and Radiative Transfer

journal homepage: [www.elsevier.com/locate/jqsrt](http://www.elsevier.com/locate/jqsrt)

## Low-frequency contributions in the radiative efficiencies of HFC-236fa, HFC-245fa and HFC-43-10mee over the 225–298 K temperature range<sup>☆</sup>

Daniela Alvarado-Jiménez<sup>a,b,c</sup>, Nicola Tasinato<sup>a</sup>,<sup>\*</sup> Richard Brownsword<sup>d</sup>,  
Damien Weidmann<sup>d</sup>, Roberto Buizza<sup>e</sup>, Keith P. Shine<sup>e</sup>,<sup>\*</sup>

<sup>a</sup> Scuola Normale Superiore, Piazza dei Cavalieri 7, Pisa, 56126, Italy<sup>b</sup> IUSS Scuola Universitaria Superiore Pavia, Piazza della Vittoria 15, Pavia, 27100, Italy<sup>c</sup> University of Reading, Whiteknights, Reading, RG6 7ET, United Kingdom<sup>d</sup> Space Science & Technology Department, STFC Rutherford Appleton Laboratory, Harwell Campus, Didcot, Oxfordshire, OX11 0QX, United Kingdom<sup>e</sup> Sant'Anna School of Advanced Studies, Piazza Martiri della Libertà 33, Pisa, 56127, Italy

## ARTICLE INFO

Dataset link: <https://doi.org/10.5286/edata/58>

## Keywords:

Infrared absorption cross sections  
Climate metrics  
Global warming  
Halogenated organics  
Quantum chemical calculations

## ABSTRACT

Hydrofluorocarbons (HFCs) are used as substitutes for ozone-depleting substances regulated under the Montreal Protocol. While having zero ozone depletion potential, HFCs strongly absorb infrared (IR) radiation, making them potent greenhouse gases. Vibrational modes associated with C–F stretching absorb strongly within the atmospheric window (750–1250 cm<sup>-1</sup>), contributing substantially to radiative forcing. The low-frequency region (< 500 cm<sup>-1</sup>), which accounts for approximately 16% of the Earth's thermal emission, has however remained largely unexplored mainly due to instrumental challenges. Here, we present the first experimental measurements of IR absorption cross-sections in the 150–500 cm<sup>-1</sup> range for HFC-236fa, HFC-245fa, and HFC-43-10mee — three industrially relevant compounds with high global warming potentials (GWPs). The spectra were recorded at the Rutherford Appleton Laboratory using a high-resolution Fourier-transform infrared (FTIR) spectrometer in the temperature range between 225 and 298 K at resolution of 0.25 cm<sup>-1</sup>. In addition, IR cross section spectra were simulated through quantum chemical (QC) calculations including a non-empirical treatment of anharmonic effects.

From the experimental results, we derived effective radiative efficiencies (EREs) in the low-frequency region of 0.001, 0.005, and 0.003 W m<sup>-2</sup> ppb<sup>-1</sup> for HFC-236fa, HFC-245fa, and HFC-43-10mee, respectively, and revised global warming potentials over 20-, 100-, and 500-year time horizons. Comparison with values reported in the WMO Ozone Assessment Report 2022 reveals minor differences for HFC-245fa and HFC-43-10mee, whereas their value for HFC-236fa shows a significant overestimation, corresponding to a discrepancy of approximately 360 units in the 100-year GWP. Theoretical predictions reproduced experimental band strengths with an overall average deviation of 4%, confirming the reliability of the computational approach even in the low-frequency region. This indicates that the QC technique is likely to provide reliable estimates for RE and GWP for similar compounds where measurements are not available.

These findings highlight that small variations in the treatment of low-frequency absorptions can propagate into substantial contributions in climate metrics, particularly for long-lived compounds. Overall, this study provides a consistent experimental–theoretical framework for quantifying the radiative forcing of HFCs and similar compounds and reduces current uncertainties in the estimation of their climate-relevant parameters.

<sup>☆</sup> This article is part of a Special issue entitled: ‘Memorial issue in honor of Mikhail Tretyakov’ published in Journal of Quantitative Spectroscopy and Radiative Transfer.

<sup>\*</sup> Corresponding authors.

E-mail addresses: [nicola.tasinato@sns.it](mailto:nicola.tasinato@sns.it) (N. Tasinato), [k.p.shine@reading.ac.uk](mailto:k.p.shine@reading.ac.uk) (K.P. Shine).

<https://doi.org/10.1016/j.jqsrt.2026.109908>

Received 12 December 2025; Received in revised form 20 February 2026; Accepted 9 March 2026

Available online 10 March 2026

0022-4073/© 2026 The Authors. Published by Elsevier Ltd. This is an open access article under the CC BY-NC-ND license (<http://creativecommons.org/licenses/by-nc-nd/4.0/>).

## 1. Introduction

Hydrofluorocarbons (HFCs) are synthetic compounds introduced as substitutes for ozone-depleting substances regulated under the Montreal Protocol [1]. They are mainly used in fire suppression, foam production, refrigeration and air conditioning, and while they do not deplete stratospheric ozone, their strong infrared (IR) absorptions makes them potent greenhouse gases, with steadily increasing atmospheric concentrations in recent decades [2]. Indeed, the presence of C–F bonds leads to intense IR absorptions within the atmospheric window ( $750\text{--}1250\text{ cm}^{-1}$ ), where relatively few other natural gases absorb efficiently. This spectral placement enhances their greenhouse capacity, and despite their low atmospheric mixing ratios, HFCs are making a growing contribution to global radiative forcing, being currently around 2% [3]. Two key climate metrics are used to quantify this effect: the effective radiative efficiency (ERE), defined as the radiative forcing per unit change in mole fraction, and the global warming potential (GWP), which compares the integrated forcing of a unit mass emission of a gas relative to an equal mass emission of  $\text{CO}_2$  over a selected time horizon. In addition to atmospheric lifetime, IR absorption cross-section data is required to determine EREs and GWPs. Recent attention has focused on the low-frequency IR region ( $< 500\text{ cm}^{-1}$ ), which accounts for nearly 16% of the terrestrial emission spectrum [4–6]. However, the great majority of Fourier-transform infrared (FTIR) measurements extend only down to  $\sim 500\text{ cm}^{-1}$ , leaving the lower spectral range largely unexplored due to instrumental challenges, particularly for the spectral region below  $400\text{ cm}^{-1}$  [7,8].

To fill this gap, in the absence of experimental data, quantum chemical (QC) calculations can be exploited to provide both IR absorption cross sections [9] and atmospheric lifetimes [10,11] required to determine climate metrics. To this end, density functional theory (DFT) within the double-harmonic approximation has been employed to estimate the contribution of low-frequency bands, which is generally predicted to be less than 5% of the total absorption cross section [6, 12,13]. However, harmonic calculations are known to overestimate vibrational frequencies and band intensities while neglecting overtones and combination bands, resulting in deviations that may range from  $\sim 20\%$  to nearly  $50\%$ , depending on the molecule [14–18].

In this context, HFC-236fa ( $\text{CF}_3\text{CH}_2\text{CF}_3$ , 1,1,1,3,3,3-hexafluoropropane), HFC-245fa ( $\text{CF}_3\text{CH}_2\text{CHF}_2$ , 1,1,1,3,3-pentafluoropropane), and HFC-43-10mee ( $\text{CF}_3\text{CF}_2\text{CHFCHFCF}_3$ , 1,1,1,2,2,3,4,5,5,5-decafluoropentane) are of particular interest due to their widespread industrial use. HFC-236fa is primarily employed in fire suppression and refrigeration, HFC-245fa as a blowing agent for foams, and HFC-43-10mee mainly as an industrial solvent. Despite their relatively low atmospheric concentrations, their high 100-year GWPs (9120, 1610, and 966 for HFC-236fa, HFC-245fa, and HFC-40-10mee, respectively) make them potentially significant contributors to global warming in the future [19]. As such, their emissions can be included in the Nationally Determined Contributions submitted by Parties to the 2015 Paris Agreement to the United Nations (UN) Framework Convention on Climate Change, and they are specifically included in the control measures of the 2016 Kigali Amendment to the UN Montreal Protocol on Substances that Deplete the Ozone Layer. Observations from the Advanced Global Atmospheric Gases Experiment (AGAGE) indicate that their atmospheric abundances have steadily increased over the past two decades [2]: HFC-236fa, the second longest-lived and highest-GWP HFC after HFC-23, increased from below 0.1 ppt in the mid-2000s to about 0.3 ppt in 2024; HFC-245fa rose from 0.7 ppt in 2007 to 3.8 ppt in 2024; and HFC-43-10mee, grew from 0.2 ppt in 2010 to approximately 0.3 ppt in 2024.

Existing literature on the ERE of these molecules is summarized in Hodebrog et al. [20] and further reported in the *Assessment of Ozone Depletion: 2022* released by the World Meteorological Organization (WMO) [19]. These ERE values are based on the mean of a collection of IR absorption cross sections spanning the  $600\text{--}1500\text{ cm}^{-1}$  range for

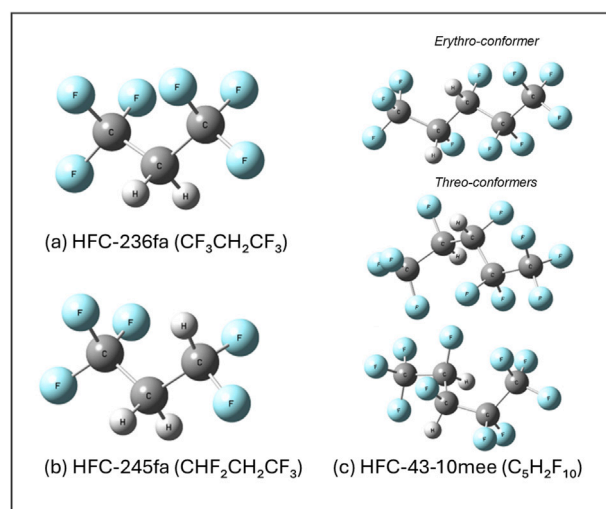


Fig. 1. Molecular structures of (a) HFC-236fa, (b) HFC-245fa, and (c) HFC-43-10mee *erythro*- and *threo*-conformers considered in this work.

HFC-236fa,  $455\text{--}1500\text{ cm}^{-1}$  for HFC-245fa, and  $500\text{--}3000\text{ cm}^{-1}$  for HFC-43-10mee. However, despite their growing climatic relevance, no experimental absorption cross sections have been reported for these molecules in the low-frequency region, which is important for fully assessing their potential climate impact.

In this study, we present the first experimental measurements of the IR absorption cross sections in the  $150\text{--}500\text{ cm}^{-1}$  range for HFC-236fa, HFC-245fa, and HFC-43-10mee, whose molecular structures are shown in Fig. 1. HFC-43-10mee presents both *erythro*- and *threo*-structural isomers, which come with a variety of conformers with the most stable ones reported in Fig. 1. The spectra are obtained at the Rutherford Appleton Laboratory (RAL) using a Bruker IFS 125 high-resolution FTIR spectrometer set to a  $0.25\text{ cm}^{-1}$  resolution. Spectra are measured at four different temperatures within the atmospheric range between 225 K and 298 K. The obtained IR absorption cross sections are employed to derive updated EREs and 20-, 100-, and 500-year GWPs for the three molecules, highlighting the relative contribution of the low-frequency region to their overall value. Experimental measurements are complemented by *in silico* predictions of climate metrics performed by adopting a recently proposed computational workflow, which integrates DFT calculations with non-empirical anharmonic corrections and conformational searches [9]. This approach has been shown to yield deviations within  $\sim 5\%$  from experiment for halogenated species, and its application to HCFC-132b demonstrated quantitative agreement with experimental measurements even in the low-frequency region [8]. A prime purpose for presenting the QC calculations is to assess the extent to which they would be applicable to other similar species where experimental measurements are not available. Overall, the results presented here provide a more consistent framework for quantifying the climate impact of these HFCs and narrowing existing gaps in their assessment.

## 2. Experimental details

Spectra were recorded using the RAL High-resolution Spectroscopy Facility's Bruker IFS 125 HR interferometer (referred to as the IFS), capable of an unapodised lineshape full-width-half-maximum (FWHM) of  $0.001\text{ cm}^{-1}$ . The IFS was configured with a 6-micron thick Mylar beamsplitter, a DTGS (deuterated L-alanine doped triglycine sulphate) pyroelectric detector with a specific detectivity of  $D^* 4 \times 10^8\text{ cm Hz}^{-1/2}\text{ W}^{-1}$  equipped with a caesium iodide window, and a conventional 'Globar' thermal IR source. The sample cell was fitted with 1-mm thick, 47 mm diameter, high-density polyethylene windows manufactured in-house. The far-IR spectral window afforded by the combined optical

chain, defined as the region in which relative response was  $> 0.95$ , was  $130\text{--}670\text{ cm}^{-1}$ . The IFS was operated under a  $0.04\text{ hPa}$  vacuum to suppress interfering absorption by atmospheric water vapour in the instrument body.

The sample cell was inserted inside the dedicated sample compartment of the IFS, with feed-throughs for gas filling and liquid cooling. The cell was made of stainless steel and had an optical path length of  $261.2 \pm 0.7\text{ mm}$ . A welded helical tube allowed the cell body to be cooled by circulation of ethanol supplied from a Julabo F95-SL refrigerated circulator. The cell temperature was measured at four points along the cell body using platinum resistance thermometers with a combined accuracy of  $\pm 2\text{ K}$ . The cell could be cooled down to  $225\text{ K}$ . Cell pressure was measured using a set of three calibrated MKS Baratron pressure transducers (1, 10 and 1000 Torr range) with a relative measurement accuracy of typically  $0.6\text{ per mil}$ .

The HFC samples were manufactured by Synquest Laboratories Inc. with a stated purity of  $97\%$  and were used without further purification. Sample mixtures were composed of HFC with partial pressures in the range  $2\text{--}200\text{ Torr}$  mixed with zero air (BOC 270028-L) to total pressures of  $100, 500$  and  $1000\text{ mbar}$ .

Transmission spectra were recorded to a maximum optical path difference of  $3.6\text{ cm}$ , which with Norton-Beer (Medium) apodization resulted in an instrumental lineshape with a FWHM of  $0.23\text{ cm}^{-1}$ . The Norton-Beer apodization function was chosen as it gives the best adherence to the Beer–Lambert law at the moderate resolution used here [21]. Measurements were recorded in sets at a given temperature and total pressure. Each transmission spectrum resulted from the average of  $100$  interferometer mirror scans to improve signal-to-noise ratio (SNR). This settings were adopted with the purpose of obtaining a resolution to SNR trade-off favouring the SNR.

To determine transmittance spectra, the experimental transmission spectra must be normalized to the overall response of the spectrometer in the absence of the sample. To do so, the measurement protocol was established as the following: (i) the sample cell was filled with zero air at the target mixture pressure and a measurement is taken, (ii) the sample cell is subsequently filled with a succession of dilute HFC/air mixtures and their spectra measured, (iii) lastly, another zero air measurement, identical to the first step is conducted. The whole series at a given temperature and pressure typically takes  $4\text{--}5\text{ h}$ .

The first zero air spectrum was taken as the background transmission spectrum to which all succeeding spectra of the set were normalized to produce transmittance spectra of the HFC samples. The transmittance root-mean-square noise achieved at peak transmission was typically  $0.002$ , representing a signal to noise ratio of  $500$ . The second zero air background spectrum, is used to evaluate the background variation occurring over the duration of the measurement. Variations of up to  $0.2$  transmittance units have been observed; in some rare occasions, measurement series were repeated in cases of large background variations greater than  $0.2$ . These resulted in a systematic baseline shift that was corrected before proceeding with spectral analysis.

All the instrumental transmission data recorded are available as ASCII files from the data repository (<https://doi.org/10.5286/edata/958>), including metadata text files listing the experimental conditions.

The photo-absorption cross-section spectrum was obtained following a well-established procedure [22–25]. Briefly, for a given temperature, the wavenumber-dependent molecular absorption cross-section spectrum ( $\text{cm}^2\text{ molecule}^{-1}$ ),  $\sigma(\bar{\nu})$ , was obtained at each pressure from the measured absorbance according to Eq. (1):

$$\sigma(\bar{\nu}) = \frac{\ln(10) A(\bar{\nu})}{N_A c l} \quad (1)$$

where  $A(\bar{\nu})$  is the absorbance at wavenumber  $\bar{\nu}$ ,  $l$  (cm) is the optical path length,  $c$  ( $\text{mol cm}^{-3}$ ) is the sample concentration, and  $N_A$  is Avogadro's number. Before proceeding to the evaluation of the absorption cross section spectra, residual absorptions from water vapour ro-vibrational transitions, not completely eliminated by normalization

to the background spectra, were removed and possible drifts in the base-line were further adjusted so that regions of no absorption resulted in total transmission of the radiation.

At each wavenumber, the final spectrum was obtained by averaging the cross sections at a given temperature across all investigated sample pressures which were scaled according to the stated sample purity. Linearity of the Beer–Lambert's Law was checked by plotting the peak absorbance of the strongest bands in the spectral region considered against the sample pressure. In all cases, a linear dependence was observed over the whole pressure range. Absorption cross sections were measured in the ranges  $155\text{--}585\text{ cm}^{-1}$  for HFC-236fa,  $135\text{--}600\text{ cm}^{-1}$  for HFC-245fa, and  $150\text{--}600\text{ cm}^{-1}$  for HFC-43-10mee.

Following the method proposed by Nemtchinov and Varanasi [26], the experimental uncertainty in the retrieved IR absorption cross section,  $\sigma$ , was evaluated by accounting for several sources of experimental error. These include uncertainties in temperature ( $T$ ), pressure ( $P$ ), and optical path length ( $l$ ), as well as the signal-to-noise ratio of the recorded spectral transmittance and the purity of the absorbing sample. The combined relative uncertainty in  $\sigma$  can be expressed as:

$$\frac{\delta\sigma(\bar{\nu})}{\sigma(\bar{\nu})} = \left\{ \left( \frac{1}{\ln \tau(\bar{\nu})} \right)^2 \left( \frac{\delta\tau(\bar{\nu})}{\tau(\bar{\nu})} \right)^2 + \left( \frac{\delta P}{P} \right)^2 + \left( \frac{\delta\xi}{\xi} \right)^2 + \left( \frac{\delta l}{l} \right)^2 \right\}^{1/2} \quad (2)$$

where  $\tau(\bar{\nu})$  is the spectral transmittance at the wavenumber  $\bar{\nu}$ ,  $P$  is the total pressure of the gas mixture,  $\xi$  is the volumetric (or molar) mixing ratio of the absorbing species, and  $l$  is the optical path length through the absorption cell;  $\delta\tau(\bar{\nu})$ ,  $\delta P$ ,  $\delta\xi$ , and  $\delta l$  represent the respective uncertainties;  $\sigma(\bar{\nu})$  denotes the absorption cross-section at wavenumber  $\bar{\nu}$ , and  $\delta\sigma(\bar{\nu})$  its corresponding uncertainty.

### 3. Computational details

The longwave radiative properties of the target molecules were investigated using a QC framework based on DFT which was described previously [8,9] and is only summarized here. EREs of HFC-236fa and HFC-245fa were calculated following the methodology developed by Alvarado and Tasinato [9], employing the double-hybrid functional DSD-PBEP86 [27] combined with the jun-cc-pVTZ [28] basis set for both molecules. For the HFC-43-10mee molecule, a hybrid force-field approach [29–31] was adopted to limit the computational cost. Specifically, equilibrium geometry, harmonic vibrational wavenumbers and IR intensities were evaluated at the DSD-PBEP86/jun-cc-pVTZ level of theory, while anharmonic contributions were computed using the meta-hybrid PW6B95 [32] density functional in combination with the jul-cc-pVTZ [28] basis set, which has been shown to provide a good trade-off between accuracy and computational cost in the prediction of climate metrics [9].

To avoid low overlap between the normal modes computed at the DSD-PBEP86 and PW6B95 levels of theory, cubic- and quartic-semidiagonal derivatives of the potential energy, as well as second- and third-order derivatives of the dipole moment surface, were evaluated at the PW6B95/jul-cc-pVTZ level by displacing atoms along the DSD-PBEP86 normal modes. While full anharmonic computations at the DSD-PBEP86/jun-cc-pVTZ and PW6B95/jul-cc-pVTZ levels of theory have been shown to be accurate for this type of application [8,9,33], this is the first time that a hybrid force-field approach has been used for climate-metric determination. Both functionals were always augmented for dispersion correlation effects by using Grimme's DFT-D3 scheme in conjunction with Becke–Johnson damping [34,35].

For molecules with multiple torsional degrees of freedom, such as HFC-43-10mee, an extensive conformational search was required. The conformational landscape was first explored using the CREST program [36] at the GFN2-xTB [37] level. Candidate conformers were then re-optimized and subjected to harmonic vibrational frequency calculations at the DSD-PBEP86/jun-cc-pVTZ level. After refinement, only conformers within  $2\text{ kcal mol}^{-1}$  from the lowest-energy structure were retained for the subsequent anharmonic spectral simulation. For

**Table 1**

Equilibrium rotational constants of HFC-236fa, HFC-245fa and HFC-43-10mee (MHz) computed at the DSD-PBEP86/jun-cc-pVTZ level of theory for the studied HFCs.

Molecule	HFC-236fa	HFC-245fa	HFC-43-10mee		
			Erythro	Threo-1	Threo-2
$A_e$	2908.277	3691.439	1205.633	1129.447	1109.131
$B_e$	1062.210	1247.752	337.687	397.193	377.797
$C_e$	1047.661	1141.717	330.263	352.319	361.560

HFC-43-10mee, three conformers – one with the *erythro* configuration and two with the *threo* configuration (see Fig. 1) – met the selection criterion and were used to simulate the overall spectral bandshape. By contrast, for HFC-245fa, although two conformations (having point group symmetry  $C_1$  and  $C_s$ ) exist, only the  $C_1$  conformer was considered in the QC simulations, since the  $C_s$  conformation exhibits a negligible Boltzmann population in the range of temperatures considered in this work.

#### 4. Results and discussion

Among the three HFCs considered in the present work, HFC-236fa is a nearly prolate asymmetric rotor, with an asymmetry parameter  $\kappa = -0.98$ , belonging to the  $C_{2v}$  symmetry point group. The most stable conformer of HFC-245fa is an asymmetric rotor ( $\kappa = -0.91$ ), with no elements of symmetry. Finally, the conformers of HFC-43-10mee all belong to the  $C_1$  symmetry point group; both *threo* structures behave as nearly prolate asymmetric rotors ( $\kappa = -0.98$ ), whereas the *erythro* conformer is more asymmetric, with  $\kappa = -0.88$ . The equilibrium rotational constants of the three molecules, computed at the DSD-PBEP86/jun-cc-pVTZ level of theory, are reported in Table 1.

##### 4.1. Experimental determination of infrared absorption cross sections

Molecules with relatively large molecular weights exhibit small rotational constants and, consequently, large moments of inertia, which in turn lead to a high density of rotational–vibrational transitions. In addition, they present a number of low-energy vibrational levels significantly populated at room temperature. As a result, their IR absorption spectra are characterized by broad, overlapping bands arising from the superposition of numerous individual transitions, including fundamental, combination, and hot bands.

The spectral congestion makes it challenging to obtain precise line shapes or to perform a line-by-line analysis of transition strengths [38–41]. For the molecules studied here, particularly in the case of HFC-43-10-mee, which presents multiple conformers, the density of transitions is sufficiently high that it is not possible to isolate individual lines or to distinguish P-, Q-, and R- branches within certain absorption bands. In such cases, rather than attempting to extract individual line parameters [38–41], the practical approach is to integrate the IR absorption cross-section spectrum to derive integrated band strengths and report the integrated intensity,  $S$ , over a defined wavenumber interval: [23–25,31,42,43].

$$S = \int_{\tilde{\nu}_1}^{\tilde{\nu}_2} \sigma(\tilde{\nu}) d\tilde{\nu} \quad (3)$$

where  $\sigma(\tilde{\nu})$  is the absorption cross-section spectrum, as defined in Eq. (1), and the integrated band strength, which in principle depends on both temperature and column density, is obtained between the integration limits  $\tilde{\nu}_1$  and  $\tilde{\nu}_2$ , corresponding to points of negligible absorption.

As illustrated in Fig. 2(a), the experimental low-frequency spectrum of HFC-236fa can be divided into three integration ranges: 285–350  $\text{cm}^{-1}$ , 365–420  $\text{cm}^{-1}$ , and 465–585  $\text{cm}^{-1}$ . According to the anharmonic QC calculations performed in this work, the first interval hosts

the absorptions of the  $\nu_8$  (330  $\text{cm}^{-1}$ ) and  $\nu_{27}$  (299  $\text{cm}^{-1}$ ) fundamentals, corresponding to CCF bending and CCF bending mixed with  $\text{CH}_2$  wagging, respectively. The spectral region between 365 and 420  $\text{cm}^{-1}$  is dominated by the  $\nu_{19}$  (395  $\text{cm}^{-1}$ ) fundamental, corresponding to a  $\text{CH}_2$  rocking vibration. The upper range, extending from 465 to 585  $\text{cm}^{-1}$ , displays several distinct features associated with the  $\nu_7$  (521  $\text{cm}^{-1}$ ),  $\nu_{18}$  (534  $\text{cm}^{-1}$ ), and  $\nu_{26}$  (539  $\text{cm}^{-1}$ ) modes. The  $\nu_7$  and  $\nu_{18}$  vibrations correspond to  $\text{CF}_2$  scissoring and rocking vibrations, respectively. The  $\nu_{26}$  mode is primarily characterized by the  $\text{CF}_2$  scissoring motion of both  $\text{CF}_3$  groups.

In Fig. 2(b), the experimental IR absorption cross-section spectrum of HFC-245fa also reveals three frequency domains, spanning the 135–185  $\text{cm}^{-1}$ , 285–405  $\text{cm}^{-1}$ , and 430–600  $\text{cm}^{-1}$  ranges. The lowest one features the  $\nu_{25}$  (154  $\text{cm}^{-1}$ ) fundamental, assigned to CCF bendings. The subsequent interval encompasses the  $\nu_{22}$  (369  $\text{cm}^{-1}$ ),  $\nu_{23}$  (337  $\text{cm}^{-1}$ ), and  $\nu_{24}$  (303  $\text{cm}^{-1}$ ) bands, associated with  $\text{CH}_2$  rocking, CCF bending, and  $\text{CF}_2$  twisting motions, respectively. Finally, the highest portion of the spectrum is characterized by absorptions of the  $\nu_{18}$  (575  $\text{cm}^{-1}$ ),  $\nu_{19}$  (557  $\text{cm}^{-1}$ ),  $\nu_{20}$  (536  $\text{cm}^{-1}$ ), and  $\nu_{21}$  (480  $\text{cm}^{-1}$ ) fundamentals. The  $\nu_{18}$  mode corresponds to a  $\text{CH}_2$  rocking vibration,  $\nu_{19}$  to a  $\text{CF}_2$  scissoring vibration, while the last two fundamentals are associated with rocking motions of the  $\text{CH}_2$  group accompanied by  $\text{CF}_2$  deformations.

Finally, due to the significant spectral overlap, the low-frequency spectrum of HFC-43-10-mee, reported in Fig. 2(c), can be divided into two integration ranges: 150–330  $\text{cm}^{-1}$  and 340–500  $\text{cm}^{-1}$ . The first interval comprises the  $\nu_{33}$ – $\nu_{40}$  fundamentals, while the second (285–405  $\text{cm}^{-1}$ ) includes the  $\nu_{29}$ ,  $\nu_{30}$ ,  $\nu_{31}$ , and  $\nu_{32}$  bands. Although the absorption around 500  $\text{cm}^{-1}$  is not negligible, this integration limit was maintained to ensure consistency with previous studies on the definition of ERE for this molecule, which report data up to this wavenumber region [12,20].

Table 2 summarizes the experimentally determined integrated IR absorption cross sections obtained for HFC-236fa, HFC-245fa, and HFC-43-10-mee at temperatures of 225, 250, 275, and 295 K within the respective integration intervals over the low-frequency region. As can be seen from Table 2, although the shape of an absorption band can vary with temperature – reflecting changes in the population of rotational levels in the ground vibrational state – the obtained integrated intensities are not significantly affected by temperature variations, in agreement with previous observations for hydrocarbons [12,44,45].

In addition to temperature dependence, the effect of total pressure was also investigated by pressuring the gas samples with zero air to total pressures of 100, 500 and 1000 mbar. As detailed in Table 3, that collects the integrated band strengths determined at the different total pressure, the pressure dependence has been found to be negligible, consistent with earlier reports [14,46]. Indeed, the effect of pressurization with an optically inert buffer gas (air, in this case) is mainly to cause broadening of the underlying ro-vibrational transitions, eventually leading to their overlap. However, for relatively heavy molecules such as those considered here, this effect is marginal because the lines are already closely spaced and tend to overlap, resulting in a pressure-independent integrated intensity [47,48].

Before closing this section, it might be interesting to compare the present measurements with previous studies that partially overlap the spectral range here considered. To the best of our knowledge there are no integrated IR cross-sections reported in the literature that overlap to the present measurements for HFC-236fa and HFC-43-10mee so among the three molecules, only for HFC-245fa a comparison is possible over the 455–515  $\text{cm}^{-1}$  range, for which a value of  $19.6 \times 10^{-19}$   $\text{cm}^2 \text{molecule}^{-1}$  has been reported.[49] When integrated over the same spectral range the presently determined IR absorption spectrum yields an integrated cross section of  $24.4 \times 10^{-19}$   $\text{cm}^2 \text{molecule}^{-1}$ , with the two values overlapping within their uncertainties.

**Table 2**

Experimental integrated band strengths ( $10^{-19}$  cm molecule $^{-1}$ ) of HFC-236fa, HFC-245fa, and HFC-43-10mee at  $T = 225, 250, 275,$  and  $298$  K, and comparison with QC counterparts.<sup>a</sup>

Molecule	Integration limits (cm $^{-1}$ )	225 K	250 K	275 K	298 K	QC	Dev. Exp. - QC <sup>b</sup>
HFC-236fa	285–350	1.0 (1)	1.2 (1)	1.0 (0.1)	1.1 (1)	1.5	0.4 (36%)
	365–420	2.5 (4)	2.6 (2)	2.4 (0.2)	2.6 (2)	3.1	0.5 (19%)
	465–585	18 (3)	18 (2)	18 (2)	19 (2)	17.5	-1.5 (-7.8%)
<b>Total</b>	<b>155–585</b>	<b>22 (3)</b>	<b>22 (3)</b>	<b>23 (2)</b>	<b>24 (2)</b>	<b>22.3</b>	<b>-1.7 (-7.1)</b>
HFC-245fa	135–185	5.1 (9)	5.0 (1)	5.7 (7)	6.3 (5)	5.4	-0.9 (-14%)
	285–405	4.8 (5)	5.1 (4)	5.4 (4)	5.7 (4)	6.4	0.7 (12.2%)
	430–600	48 (5)	51 (4)	53 (4)	54 (4)	50.0	-4 (-7.4%)
<b>Total</b>	<b>135–600</b>	<b>57 (7)</b>	<b>62 (6)</b>	<b>64 (6)</b>	<b>66 (5)</b>	<b>63.2</b>	<b>-2.8 (-4.2%)</b>
HFC-43-10-mee	150–330	–	18 (4)	19 (2)	21 (1)	21.1	0.1 (0.48%)
	340–500	–	14 (4)	14 (1)	15 (1)	14.7	-0.3 (-0.13%)
	<b>Total</b>	<b>150–500</b>	<b>–</b>	<b>31 (8)</b>	<b>33 (3)</b>	<b>36 (3)</b>	<b>36.1</b>

<sup>a</sup> Figures within parentheses are experimental errors in the units of the last significant digit.

<sup>b</sup> Absolute and percentage relative (within parentheses) deviations between experimental and QC integrated band strengths.

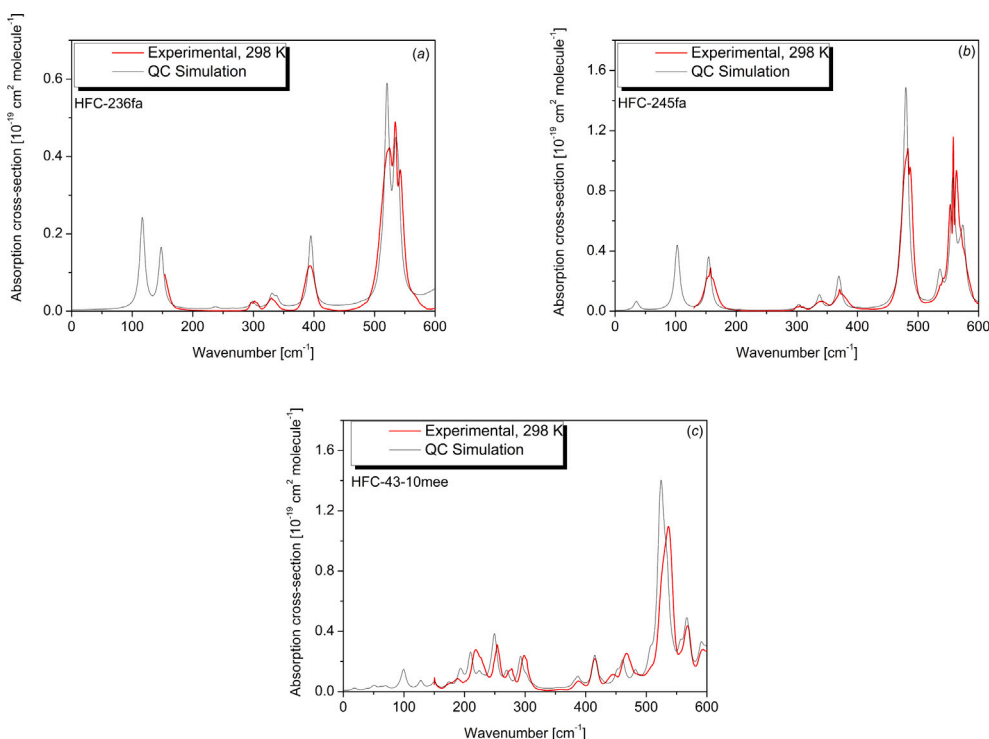


**Fig. 2.** Experimental IR photo-absorption cross-section spectrum of (a) HFC-236fa, (b) HFC-245fa, and (c) HFC-43-10mee between 150 and 600 cm $^{-1}$  ( $T = 298 \pm 0.1$  K, resolution = 0.25 cm $^{-1}$ , optical path length = 261.2  $\pm$  0.7 mm), superimposed with traces simulated by QC calculations covering the 0–600 cm $^{-1}$  range.

**Table 3**

Experimental integrated band strengths ( $10^{-19}$  cm molecule $^{-1}$ ) of HFC-236fa, HFC-245fa, and HFC-43-10mee at different total pressures.

Molecule	Integration limits (cm $^{-1}$ )	100 mbar	500 mbar	1000 mbar
HFC-236fa	285–350	0.9	0.9	1.0
	365–420	2.3	2.4	2.4
	465–585	17.4	17.5	17.4
HFC-245fa	130–185	5.2	5.3	5.0
	285–405	4.7	4.8	4.7
	430–600	47.4	47.8	46.0
HFC-43-10mee	150–330	16.4	15.9	17.2
	340–500	12.6	12.2	13.2

#### 4.2. QC prediction of infrared absorption cross sections

The experimentally measured IR absorption cross-section spectra are superimposed in Fig. 2 with the corresponding band shapes calculated through QC calculations, obtained by convoluting the computed

stick spectrum with a Lorentzian function having a half width at half maximum of 5 cm $^{-1}$ . The comparison between QC simulations and experimental spectra taken from the HITRAN database [50–52], covering the 700–1500 cm $^{-1}$  region, is shown in Fig. 3. The overall agreement between QC and experimental band shapes is very good,

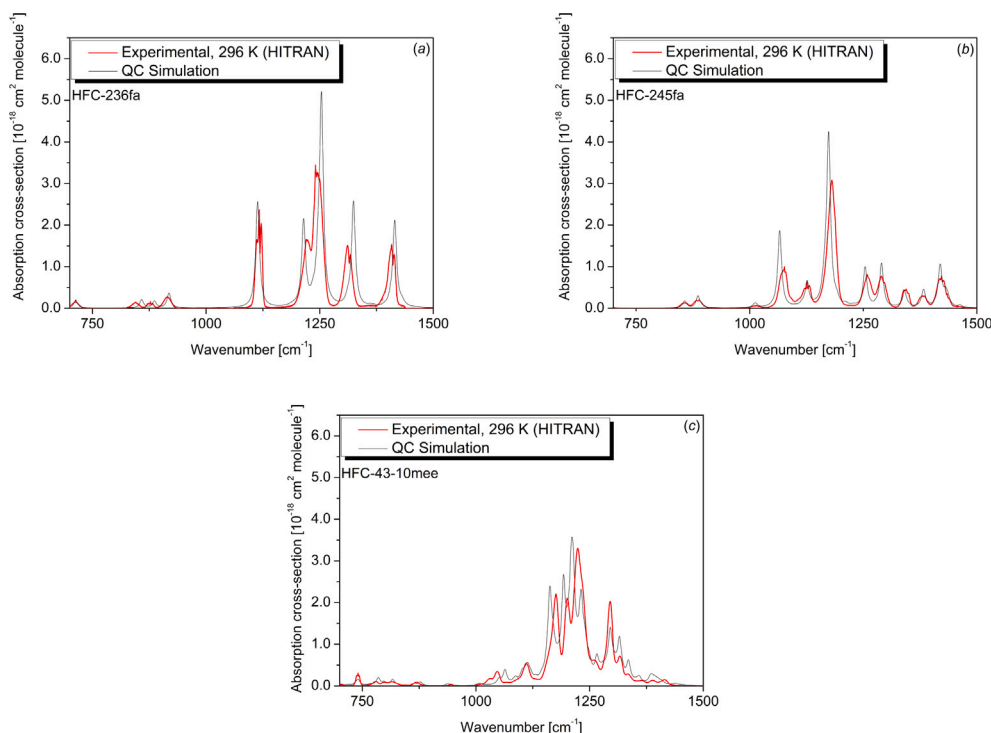


Fig. 3. Experimental IR photo-absorption cross-section spectrum of (a) HFC-236fa, (b) HFC-245fa, and (c) HFC-43-10-mee between 750 and 1500  $\text{cm}^{-1}$  taken from the HITRAN database superimposed to QC spectra simulated in this work.

with only a few frequency shifts. The small discrepancies in some peak absorbances are mainly due to the adoption of an effective broadening function instead of the full consideration of the underlying ro-vibrational envelope.

Table 2 also lists theoretical band strengths obtained by integrating simulated IR absorption cross-section spectra over the same spectral ranges as adopted in the experimental analysis. The comparison indicates that *in silico* predictions closely match experimental values: the largest deviation in relative terms is observed for HFC-236fa in the 285–350  $\text{cm}^{-1}$  spectral interval, where the experimental value is overestimated by 36%. This apparently large deviation is, however, inflated by the small integrated band intensity in this region ( $1.1 \times 10^{-19} \text{ cm molecule}^{-1}$ ); indeed, in absolute terms, the discrepancy between QC predictions and experiment is only  $0.4 \times 10^{-19} \text{ cm molecule}^{-1}$ . Overall, the mean deviations over the entire low-frequency integration range amount to about  $-7\%$  for HFC-236fa,  $-4\%$  for HFC-245fa, and  $-0.3\%$  for HFC-43-10-mee, respectively. Hence, QC estimates are in excellent agreement with the experimental data, falling within the expected uncertainty previously reported [9]. This agreement supports previous findings that the use of double-hybrid functionals and the inclusion of anharmonic effects significantly improves the accuracy of calculated transition frequencies and intensities, both for single vibrational excitations and for two-quanta transitions [53,54]. By considering the spectral range targeted experimentally, the overall anharmonic contribution stemming from overtone and combination transitions, mechanical and electrical anharmonic shifts on fundamental bands, and anharmonic couplings is between 3% and 6% depending on the molecule.

While previous theoretical studies on HFC-43-10mee pointed out that “the theoretical and experimental data do not agree so well, with the theoretical total integrated band strength being about 10% higher than its experimental counterparts” [12], the integrated band strength for the 0–550  $\text{cm}^{-1}$  frequency region was predicted to be  $0.68 \times 10^{-19} \text{ cm molecule}^{-1}$ , about 85% greater than the experimental (and QC, as well) value here determined. The superior accuracy of the present QC computations for the low-frequency region can be mainly attributed to the

use of the double-hybrid DSD-PBEP86 functional, significantly more accurate than the B3LYP global hybrid [9,29,55] and to the non-empirical inclusion of anharmonic effects. Indeed, while the double-harmonic approximation can be partially improved by using ad hoc scaling factors, these are typically effective for the specific class of molecules and spectral ranges underlying their parametrization and their portability to other compounds or even different spectral regions is not guaranteed.

Preliminary results here obtained for HFC-236fa and HFC-245fa show that when the same procedure as proposed in Ref. [56], and based on scaled harmonic computations using the B3LYP/6-31G\*\* method [57,58], is applied to the frequency region below about 400  $\text{cm}^{-1}$  it produces positive frequency shifts, up to 11  $\text{cm}^{-1}$  (with a turnover behaviour around 500  $\text{cm}^{-1}$ ) while actual anharmonicity usually produces a negative shift. Furthermore, if the scaling is applied to the C–Cl stretching vibrations of HCFC-132b, the B3LYP harmonic frequencies move from 785 and 748  $\text{cm}^{-1}$  to 779 and 743  $\text{cm}^{-1}$ , respectively, resulting in a worse agreement with experimental wavenumbers measured at 786 and 768  $\text{cm}^{-1}$  [8]. For comparison, anharmonic computations at the DSD-PBEP86 level predict them at 785 and 768  $\text{cm}^{-1}$ .

#### 4.3. Climate metrics

The ERE and GWP, key metrics to assess the climate impact of weak absorbers such as HFC-236fa, HFC-245fa, and HFC-43-10mee, have been derived from IR absorption cross-section data. Within this framework, the low-frequency IR region ( $< 500 \text{ cm}^{-1}$ ) plays a non-negligible role [4–6], yet it is often neglected in such evaluations. As an example, Fig. 4 illustrates this contribution for HFC-245fa by showing the experimentally measured IR absorption cross-section spectrum superimposed on the global-mean radiative forcing due to a weak absorber acting at all wavenumbers calculated by Shine and Myhre [59]. In this figure, the low-frequency IR absorption cross section (red trace) has been experimentally measured in this work, while the portion from 600 to 1500  $\text{cm}^{-1}$  has been taken from the HITRAN database [50–52].

**Table 4**  
ERE ( $\text{W m}^{-2} \text{ ppb}^{-1}$ ) of HFC-236fa, HFC-245fa, and HFC-43-10-mee.

Molecule	RE low freq. (Exp.) <sup>a</sup>	RE low freq. (QC) <sup>b</sup>	Low freq. contrib. (Exp.) <sup>a</sup>	Low freq. contrib. <sup>c</sup>	ERE (Exp.) <sup>d</sup>
HFC-236fa	0.0009	0.0008	0.3%	4.8%	0.252
HFC-245fa	0.0050	0.0048	1.9%	2.8%	0.249
HFC-43-10-mee	0.0031	0.0030	0.8%	0.5%	0.361

<sup>a</sup> From experimental IR absorption cross-sections.

<sup>b</sup> From QC IR absorption cross sections computed in the present work.

<sup>c</sup> From Ref. [6].

<sup>d</sup> From RE values taken from the WMO [19], for the spectra above  $500 \text{ cm}^{-1}$  increased with low frequency contribution determined experimentally in the present work.

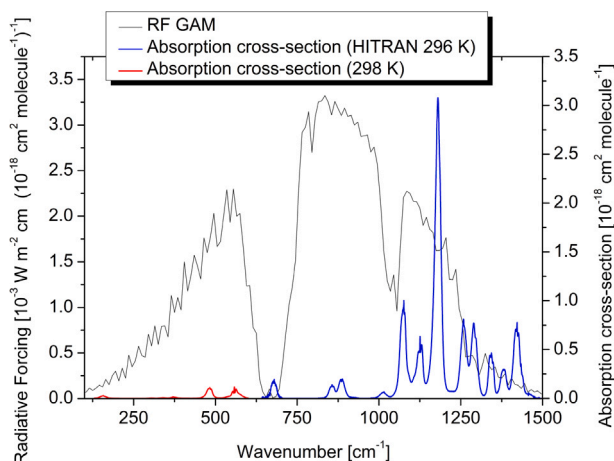


**Fig. 4.** Experimental IR absorption cross-section spectrum of HFC-245fa superimposed with the global-mean radiative forcing due to a weak absorber acting at all wavenumbers.

Radiative Efficiencies (REs) have been calculated using the method proposed by Pinnock et al. [60] according to the following equation:

$$RE = \sum_{i=1}^N F_{\sigma}^i \int_{\tilde{\nu}_{i,1}}^{\tilde{\nu}_{i,2}} \sigma(\tilde{\nu}) d\tilde{\nu} \quad (4)$$

where  $F_{\sigma}^i$  represents the global-mean radiative forcing per unit cross section due to a weak absorber within spectral interval  $i$ , from  $\tilde{\nu}_{i,1}$  to  $\tilde{\nu}_{i,2}$  and  $\sigma_i$  is the IR cross section spectrum integrated over the same range. In our calculations, we adopted the radiative forcing values reported by Shine and Myhre [59], which include the impact of stratospheric temperature adjustment on the forcing, sampled in  $10 \text{ cm}^{-1}$  wide bins. The Pinnock method assumes a uniformly mixed gas distribution with respect to altitude and latitude; however, when this assumption does not hold, a correction for the atmospheric lifetime ( $\tau$ ) should be applied [20]. In this study, RE values have been adjusted taking the most recent lifetimes of HFC-236fa (213 years), HFC-245fa (7.74 years), and HFC-43-10-mee (17 years) from the latest WMO Ozone Assessment Report [19], within the S-shaped curve [61], under the assumption that OH oxidation represents the dominant atmospheric sink. Finally, to produce the ERE favoured by the Intergovernmental Panel on Climate Change [3] (as it is regarded as a better predictor of surface temperature response) a further change to the RE should be applied to account for tropospheric adjustments; as noted in Ref. [3] (Section 7.3.2.4) such adjustments are not yet available for the species considered here. Following Forster, et al. [3], these are therefore assumed to be  $0 \pm 13\%$ .

In addition to using the data measured experimentally in this work, EREs were also derived from quantum-chemically simulated IR absorption cross-sections following the recently validated workflow of Alvarado-Jiménez and Tasinato [9]. Table 4 reports the EREs due to the low-frequency region, along with the total ERE, which includes the contribution from the low-frequency region to the mid-IR range. According to Hodnebrog et al. [61], the calculation of ERE involves

several sources of uncertainty: 5% from the radiation scheme, 5% due to cloud effects, 3% from the distribution of water vapour, 3% associated with surface and atmospheric temperatures, 5% from the tropopause height, 1% from temporal and spatial averaging, and an additional contribution from the absorption cross sections. As noted above, there is then an additional uncertainty due to the tropospheric adjustments estimated to be 13% [3].

Table 4 also includes QC EREs: as can be observed, theoretical calculations are in excellent agreement with experimental data, showing differences of only -3% for both HFC-245fa and HFC-236fa, and -5% for HFC-43-10-mee, well within the experimental uncertainty. Important attention should be paid to the good agreement between theory and experiment for HFC-43-10-mee, which provides good evidence of the effectiveness of using the hybrid DSD:PW6 force field in the prediction of climate metrics. This approach retains the accuracy of DSD-PBEP86/jun-cc-pVTZ for harmonic properties but employs the computationally less demanding PW6B95 hybrid functional for the evaluation of higher-order derivatives.

The low-frequency EREs obtained here (both experimental and theoretical) can be compared with those previously estimated based on harmonic calculation carried out at the  $\omega$ B97X-D/def2-TZVPPD level of theory [6], as also shown in Table 4. While a low-frequency contribution of about 0.5% can be confirmed in the case of HFC-43-10-mee, differences are noted for HFC-236fa and HFC-245fa. In the case of HFC-236fa, the spectral region below  $500 \text{ cm}^{-1}$  was previously estimated to contribute approximately 5% to the total ERE, while in the present work, it leads to a contribution of just 0.3%. Similarly, a 2.8% ERE due to the low-frequency contribution was reported for HFC-245fa, but our experimental (and QC as well) measurements indicated 1.9%. To ensure that these discrepancies are not due to the  $< 100 \text{ cm}^{-1}$  spectral range, and considering the overall good agreement with our experimental data, we have also estimated the theoretical RE over the entire  $0\text{--}500 \text{ cm}^{-1}$  range. No significant changes in either RE or ERE was found on including this range. Hence, discrepancies between our experimental measurements and QC simulations on one side, and theoretical estimates reported by Van Hoomissen et al. [6] on the other, could be explained by their use of IR spectra computed under the double-harmonic approximation. Even when frequency scaling is used, this approach, while widely adopted due to its reduced computational cost, neglects purely anharmonic transitions such as overtone and combination bands, as well as the redistribution of intensity caused by vibrational couplings. As a result, it tends to overestimate the strength of the fundamental absorption bands and, consequently, the ERE. The EREs obtained from our experiments highlight the importance of including anharmonic contributions in the simulations, since purely harmonic treatments may give a misleading impression of accuracy while masking significant physical effects.

Finally, updated values of GWP of the studied molecules have been determined by using the experimental data obtained here for the low-frequency region to complement those previously reported for the spectral region above  $500 \text{ cm}^{-1}$  [19]. GWPs over the 20-, 100-, and 500-year time horizons are collected in Table 5, where they are compared with those in the WMO 2022 Ozone Assessment Report [19], in which the low-frequency region contribution was derived from the previously described harmonic DFT estimates [6]. The WMO 2022

**Table 5**  
Global Warming Potential of HFC-236fa, HFC-245fa, and HFC-43-10-mee over the 20-, 100-, and 500-year time horizons.

Molecule	This work			WMO 2022 <sup>a</sup>		
	20-yr	100-yr	500-yr	20-yr	100-yr	500-yr
HFC-236fa	7330	8340	5740	7650	8700	5990
HFC-245fa	3080	908	259	3110	910	260
HFC-43-10-mee	3890	1530	437	3880	1520	440

<sup>a</sup> From Ref. [19] by excluding the climate-carbon feedback term.

GWPs include the impact of the complicated and uncertain climate-carbon feedback term. For a cleaner comparison, we present the WMO 2022 results derived without this feedback (i.e. calculated directly from the WMO 2022 values for adjusted ERE and atmospheric lifetime) and use their stated values for the CO<sub>2</sub> absolute global warming potential.

Results for GWPs mirror those obtained for EREs: while no substantial differences can be noted for HFC-43-10-mee, the GWPs of HFC-245fa presented in the WMO report appear slightly overestimated, as was the low-frequency contribution to the RE. As expected, the WMO value of the 100-year GWP of HFC-236fa is overestimated by about 4.4%, again reflecting the overestimation of the low-frequency contribution in the RE. In this case, it differs by about 360 units, which is substantial considering its long atmospheric lifetime. These findings are particularly relevant because the GWP depends on both the atmospheric lifetime and the ERE of a compound. Although the contribution of the low-frequency region to the ERE accounts for only a few percent, deviations in this spectral range can significantly influence the GWP when the molecule is highly persistent in the atmosphere. This is especially true for HFC-236fa, which has one of the longest atmospheric lifetimes among HFCs (213 years) and the second-highest GWP.

Overall, the obtained results underline the critical role of experimental measurements in strengthening the reliability of GWP estimates for HFCs and related compounds, and demonstrate that QC calculations non-empirically including all relevant physical ingredients can yield predictions consistent with the most refined experimental approaches.

## 5. Conclusions

This work presented the first experimental measurements of low-frequency IR absorption cross sections for HFC-236fa, HFC-245fa, and HFC-43-10mee, from which updated values of EREs and GWPs were derived—thus providing important datasets previously absent from climate assessments. The comparison with advanced QC simulations showed excellent agreement, confirming that the inclusion of anharmonic effects substantially improves the accuracy of predicted spectra relative to the widely used double-harmonic approximation. Our results indicate that, while the low-frequency region contributes only a few percent to the total ERE, its accurate treatment is essential, particularly for long-lived species such as HFC-236fa. In this case, the nearly 400-unit discrepancy in the 100-year GWP relative to previous estimates underscores how even modest longwave spectral contributions can propagate into significant differences in climate metrics. These findings highlight the importance of combining experimental data with refined computational protocols to ensure robust climate impact assessments of synthetic greenhouse gases. Given that experimental results of the low-frequency contribution are not available for many of the species listed in WMO and IPCC assessments, the very good agreement between the measurements and the QC calculations presented here give confidence that such QC calculations can be reliably applied to similar species. We will present an extended list of such EREs in a separate publication. By narrowing existing uncertainties, this work provides a more reliable basis for future updates to international climate assessments, including those by the WMO and IPCC, and reinforces the value of integrated experimental–computational approaches in atmospheric science.

## CRedit authorship contribution statement

**Daniela Alvarado-Jiménez:** Writing – original draft, Investigation, Formal analysis. **Nicola Tasinato:** Writing – review & editing, Supervision, Software, Resources, Methodology, Funding acquisition, Conceptualization. **Richard Brownsword:** Writing – review & editing, Methodology. **Damien Weidmann:** Writing – review & editing, Resources, Methodology, Investigation. **Roberto Buizza:** Writing – review & editing. **Keith P. Shine:** Writing – review & editing, Supervision, Funding acquisition, Formal analysis, Conceptualization.

## Declaration of competing interest

The authors declare that they have no known competing financial interests or personal relationships that could have appeared to influence the work reported in this paper.

## Acknowledgements

The STARK group is acknowledged for high-performance computing facilities. Scuola Normale Superiore, Italy and IUSS Pavia, Italy are acknowledged for financial support. This publication was produced while attending the PhD programme in PhD in Sustainable Development And Climate Change at the University School for Advanced Studies IUSS Pavia, Cycle XXXVIII, with the support of a scholarship co-financed by the Ministerial Decree no. 352 of 9th April 2022, based on the NRRP - funded by the European Union – Next Generation EU - Mission 4 “Education and Research”, Component 2 “From Research to Business”, Investment 3.3. The UK Natural Environment Research Council grant InHALE (Investigating HALocarbon impacts on the global Environment) supported the contributions from the University of Reading, United Kingdom (Grant Reference NE/X004198/1) and the Rutherford Appleton Laboratory, United Kingdom (Grant Reference NE/X003558/1).

## Data availability

Data are openly available in the Science and Technology Facility Council Research Data Repository at <https://doi.org/10.5286/edata/958>.

## References

- [1] United Nations Environment Programme. The montreal protocol on substances that deplete the ozone layer. 1987.
- [2] Prinn RG, Weiss RF, Arduini J, Arnold T, DeWitt HL, Fraser PJ, Ganesan AL, Gasore J, Harth CM, Hermansen O, Kim J, Krummel PB, Li S, Loh ZM, Lunder CR, Maione M, Manning AJ, Miller BR, Mitrevski B, Mühle J, O'Doherty S, Park S, Reimann S, Rigby M, Saito T, Salameh PK, Schmidt R, Simmonds PG, Steele LP, Vollmer MK, Wang RH, Yao B, Yokouchi Y, Young D, Zhou L. History of chemically and radiatively important atmospheric gases from the advanced global atmospheric gases experiment (AGAGE). *Earth Syst Sci Data* 2018;10:985–1018. <http://dx.doi.org/10.5194/essd-10-985-2018>.
- [3] Forster P, Storelvmo T, Armour K, Collins W, Dufresne J-L, Frame D, Lunt D, Mauritsen T, Palmer M, Watanabe M, Wild M, Zhang H. The earth's energy budget, climate feedbacks, and climate sensitivity. 2021, p. 923–1054. <http://dx.doi.org/10.1017/9781009157896.009>, IPCC 6th Assess. Rep.

- [4] Harries J, Carli B, Rizzi R, Serio C, Mlynczak M, Palchetti L, Maestri T, Brindley H, Masiello G. The far-infrared Earth. *Rev Geophys* 2008;46. <http://dx.doi.org/10.1029/2007RG000233>.
- [5] Feldman DR, Collins WD, Pincus R, Huang X, Chen X. Far-infrared surface emissivity and climate. *Proc Natl Acad Sci USA* 2014;111:16297–302. <http://dx.doi.org/10.1073/pnas.1413640111>.
- [6] Van Hooymissen D, Papadimitriou VC, Burkholder JB. Low frequency (< 500 cm<sup>-1</sup>) contribution to greenhouse gas radiative efficiency. *Mol Phys* 2023;e2273412. <http://dx.doi.org/10.1080/00268976.2023.2273412>.
- [7] Beukes J, Nicolaisen F. Infrared absorption cross-sections and integrated absorption intensities for difluoromethane (HFC-32) and 1,1,1,2-tetrafluoroethane (HFC-134a) in the 650–50 cm<sup>-1</sup> region. *J Quant Spectrosc Radiat Transfer* 2000;66(2):185–98. [http://dx.doi.org/10.1016/S0022-4073\(99\)00216-2](http://dx.doi.org/10.1016/S0022-4073(99)00216-2), URL <https://www.sciencedirect.com/science/article/pii/S0022407399002162>.
- [8] Alvarado-Jiménez D, Pietropoli Charmet A, Stoppa P, Tasinato N. The radiative efficiency and global warming potential of HCFC-132b. *ChemPhysChem* 2025;26:e202400632. <http://dx.doi.org/10.1002/cphc.202400632>.
- [9] Alvarado-Jiménez D, Tasinato N. In silico modelling of radiative efficiencies of anthropogenic greenhouse gases. *Atmos Environ* 2024;338:120839. <http://dx.doi.org/10.1016/j.atmosenv.2024.120839>.
- [10] Rais N, Salta Z, Tasinato N. Thermochemistry and kinetics of the OH- and Cl-initiated degradation pathways of the HCFC-132b atmospheric pollutant. *ACS Earth Space Chem* 2023;7:892–900. <http://dx.doi.org/10.1021/acsearthspacechem.3c00025>.
- [11] Rais N, Salta Z, Tasinato N. Theoretical investigation of the OH-initiated atmospheric degradation mechanism of CX<sub>2</sub>CHX (X=H, F, Cl) by advanced quantum chemical and transition state theory methods. *Phys Chem Chem Phys* 2024;26:19976–91. <http://dx.doi.org/10.1039/D4CP01453G>.
- [12] Le Bris K, DeZeeuw J, Godin PJ, Strong K. Infrared absorption cross-sections, radiative efficiency and global warming potential of HFC-43-10mee. *J Mol Spectrosc* 2018;348:64–7.
- [13] Papanastasiou DK, Beltrone A, Marshall P, Burkholder JB. Global warming potential estimates for the C<sub>1</sub>–C<sub>3</sub> hydrochlorofluorocarbons (HCFCs) included in the Kigali amendment to the Montreal Protocol. *Atmos Chem Phys* 2018;18:6317–30. <http://dx.doi.org/10.5194/acp-18-6317-2018>.
- [14] Papasavva S, Tai S, Esslinger A, Illinger KH, Kenny JE. Ab initio calculations of vibrational frequencies and infrared intensities for global warming potential of CFC substitutes: CF<sub>2</sub>CH<sub>2</sub>F (HFC-134a). *J Phys Chem A* 1995;99:3438–43. <http://dx.doi.org/10.1021/ji00011a006>.
- [15] Young CJ, Hurley MD, Wallington TJ, Mabury SA. Molecular structure and radiative efficiency of fluorinated ethers: A structure-activity relationship. *J Geophys Res Atmos* 2008;113. <http://dx.doi.org/10.1029/2008JD010178>.
- [16] Blowers P, Hollingshead K. Estimations of global warming potentials from computational chemistry calculations for CH<sub>2</sub>F<sub>2</sub> and other fluorinated methyl species verified by comparison to experiment. *J Phys Chem A* 2009;113:5942–50. <http://dx.doi.org/10.1021/jp8114918>.
- [17] Holtomo O, Motapon O, Nsangou M. DFT study of photochemical properties and radiative forcing efficiency features of the stereoisomers cis- and trans-CHCl=CH-CF<sub>3</sub>. *J Phys Chem A* 2019;123:10437–45. <http://dx.doi.org/10.1021/acs.jpca.9b08089>.
- [18] Burkholder JB, Marshall P, Bera PP, Francisco JS, Lee TJ. Climate metrics for C1–C4 hydrofluorocarbons (HFCs). *J Phys Chem A* 2020;124(23):4793–800. <http://dx.doi.org/10.1021/acs.jpca.0c02679>.
- [19] World Meteorological Organization (WMO). *Scientific assessment of ozone depletion: 2022, GAW report no. 278*. Geneva, Switzerland: WMO; 2022.
- [20] Hodnebrog Ø, Aamaas B, Fuglestvedt JS, Marston G, Myhre G, Nielsen CJ, Sandstad M, Shine KP, Wallington TJ. Updated global warming potentials and radiative efficiencies of halocarbons and other weak atmospheric absorbers. *Rev Geophys* 2020;58. <http://dx.doi.org/10.1029/2019RG000691>, e2019RG000691.
- [21] Griffiths P, De Haseth J, Winefordner J. Fourier transform infrared spectrometry. In: *Chemical analysis: a series of monographs on analytical chemistry and its applications*, Wiley; 2007, URL [https://books.google.it/books?id=C\\_c0Gve8MX0C](https://books.google.it/books?id=C_c0Gve8MX0C).
- [22] Pietropoli Charmet A, Stoppa P, Tasinato N, Baldan A, Giorgianni S, Gambi A. Spectroscopic study of CHBrF<sub>2</sub> up to 9500 cm<sup>-1</sup>: Vibrational analysis, integrated band intensities, and ab initio calculations. *J Chem Phys* 2010;133:044310. <http://dx.doi.org/10.1063/1.3460922>.
- [23] Pietropoli Charmet A, Stoppa P, Giorgianni S, Bloino J, Tasinato N, Carnimeo I, Biczysko M, Puzzarini C. Accurate vibrational-rotational parameters and infrared intensities of 1-bromo-1-fluoroethene: A joint experimental analysis and ab initio study. *J Phys Chem A* 2017;121:3305–17. <http://dx.doi.org/10.1021/acs.jpca.7b02060>.
- [24] Stoppa P, Pietropoli Charmet A, Tasinato N, Giorgianni S, Gambi A. Infrared spectra, integrated band intensities, and anharmonic force field of H<sub>2</sub>C=CHF. *J Phys Chem A* 2009;113:1497–504. <http://dx.doi.org/10.1021/jp808556e>.
- [25] Tasinato N, Pietropoli Charmet A, Stoppa P, Giorgianni S, Gambi A. Quantum-chemical ab initio investigation of the vibrational spectrum of halon 1113 and its anharmonic force field: A joint experimental and computational approach. *Chem Phys* 2012;397:55–64. <http://dx.doi.org/10.1016/j.chemphys.2011.12.015>.
- [26] Nemtchinov V, Varanasi P. Absorption cross-sections of HFC-134a in the spectral region between 7 and 12 μm. *J Quant Spectrosc Radiat Transfer* 2004;83:285–94. [http://dx.doi.org/10.1016/S0022-4073\(02\)00356-4](http://dx.doi.org/10.1016/S0022-4073(02)00356-4).
- [27] Santra G, Sylvestry N, Martin JML. Minimally empirical double-hybrid functionals trained against the GMTKN55 database: revDSD-PBEP86-D4, revDOD-PBE-D4, and DOD-SCAN-D4. *J Phys Chem A* 2019;123:5129–43. <http://dx.doi.org/10.1021/acs.jpca.9b03157>.
- [28] Papajak E, Zheng J, Xu X, Leverentz HR, Truhlar DG. Perspectives on basis sets beautiful: Seasonal plantings of diffuse basis functions. *J Chem Theory Comput* 2011;7:3027–34. <http://dx.doi.org/10.1021/ct200106a>.
- [29] Barone V, Ceselin G, Fusé M, Tasinato N. Accuracy meets interpretability for computational spectroscopy by means of hybrid and double-hybrid functionals. *Front Chem* 2020;8:584203. <http://dx.doi.org/10.3389/fchem.2020.584203>.
- [30] Pietropoli Charmet A, Ceselin G, Stoppa P, Tasinato N. The spectroscopic characterization of halogenated pollutants through the interplay between theory and experiment: Application to R1122. *Molecules* 2022;27:748. <http://dx.doi.org/10.3390/molecules27030748>.
- [31] Tasinato N, Pietropoli Charmet A, Ceselin G, Salta Z, Stoppa P. In vitro and in silico vibrational-rotational spectroscopic characterization of the next-generation refrigerant HFO-1123. *J Phys Chem A* 2022;126:5328–42. <http://dx.doi.org/10.1021/acs.jpca.2c04680>.
- [32] Zhao Y, Truhlar DG. Design of density functionals that are broadly accurate for thermochemistry, thermochemical kinetics, and nonbonded interactions. *J Phys Chem A* 2005;109:5656–67. <http://dx.doi.org/10.1021/jp050536c>.
- [33] Melosso M, Stoppa P, Alvarado-Jiménez D, Tamassia F, Sapienza C, Bizzocchi L, Dore L, Puzzarini C, Pietropoli Charmet A, Tasinato N. Completing the spectral mosaic of chloromethane by adding the CHD<sub>2</sub>Cl missing piece through the interplay of rotational/vibrational spectroscopy and quantum chemical calculations. *Molecules* 2025;30:1604. <http://dx.doi.org/10.3390/molecules30071604>.
- [34] Grimme S, Antony J, Ehrlich S, Krieg H. A consistent and accurate ab initio parametrization of density functional dispersion correction (DFT-D) for the 94 elements H–Pu. *J Chem Phys* 2010;132:154104. <http://dx.doi.org/10.1063/1.3382344>.
- [35] Grimme S, Ehrlich S, Goerigk L. Effect of the damping function in dispersion corrected density functional theory. *J Comput Chem* 2011;32:1456–65. <http://dx.doi.org/10.1002/jcc.21759>.
- [36] Pracht P, Bohle F, Grimme S. Automated exploration of the low-energy chemical space with fast quantum chemical methods. *Phys Chem Chem Phys* 2020;22:7169–92. <http://dx.doi.org/10.1039/C9CP06869D>.
- [37] Grimme S. Exploration of chemical compound, conformer, and reaction space with meta-dynamics simulations based on tight-binding quantum chemical calculations. *J Chem Theory Comput* 2019;15:2847–62. <http://dx.doi.org/10.1021/acs.jctc.9b00143>.
- [38] Tasinato N, Stoppa P, Pietropoli Charmet A, Giorgianni S, Buffa G, Gambi A. Toward a complete understanding of the vinyl fluoride spectrum in the atmospheric region. *ChemPhysChem* 2011;12:356–63. <http://dx.doi.org/10.1002/cphc.201000859>.
- [39] Tasinato N, Pietropoli Charmet A, Stoppa P, Buffa G, Puzzarini C. A complete listing of sulfur dioxide self-broadening coefficients for atmospheric applications by coupling infrared and microwave spectroscopy to semiclassical calculations. *J Quant Spectrosc Radiat Transfer* 2013;130:233–48. <http://dx.doi.org/10.1016/j.jqsrt.2013.03.015>.
- [40] Tasinato N, Turchetto A, Puzzarini C, Stoppa P, Pietropoli Charmet A, Giorgianni S. Self-, N<sub>2</sub>-, O<sub>2</sub>-broadening coefficients and line parameters of HFC-32 for ν<sub>7</sub> band and ground state transitions from infrared and microwave spectroscopy. *Mol Phys* 2014;112:2384–96. <http://dx.doi.org/10.1080/00268976.2014.900197>.
- [41] Ceselin G, Tasinato N, Puzzarini C, Pietropoli Charmet A, Stoppa P, Giorgianni S. CO<sub>2</sub>-, He- and H<sub>2</sub>-broadening coefficients of SO<sub>2</sub> for ν<sub>1</sub> band and ground state transitions for astrophysical applications. *J Quant Spectrosc Radiat Transfer* 2017;203:367–76. <http://dx.doi.org/10.1016/j.jqsrt.2017.02.018>.
- [42] Pietropoli Charmet AP, Stoppa P, Tasinato N, Baldan A, Giorgianni S, Gambi A. Spectroscopic study of CHBrF<sub>2</sub> up to 9500 cm<sup>-1</sup>: Vibrational analysis, integrated band intensities, and ab initio calculations. *J Chem Phys* 2010;133:044310.
- [43] Pietropoli Charmet A, Ceselin G, Stoppa P, Tasinato N. The spectroscopic characterization of halogenated pollutants through the interplay between theory and experiment: Application to R1122. *Molecules* 2022;27:748. <http://dx.doi.org/10.3390/molecules27030748>.
- [44] Smith K, Newnham D, Page M, Ballard J, Duxbury G. Infrared band strengths and absorption cross-sections of HFC-32 vapour. *J Quant Spectrosc Radiat Transfer* 1996;56:73–82. [http://dx.doi.org/10.1016/0022-4073\(96\)00019-2](http://dx.doi.org/10.1016/0022-4073(96)00019-2).
- [45] Godin PJ, Johnson H, Piuanno R, Le Bris K, Strong K. Conformational analysis and global warming potentials of 1,1,1,2,3,3-hexafluoropropane and 1,1,2,2,3-pentafluoropropane from absorption spectroscopy. *J Quant Spectrosc Radiat Transfer* 2019;225:337–50. <http://dx.doi.org/10.1016/j.jqsrt.2019.01.003>.
- [46] Grosch A, Beushausen V, Wackerbarth H, Thiele O, Berg T. Temperature- and pressure-dependent midinfrared absorption cross sections of gaseous hydrocarbons. *Appl Opt* 2010;49:196. <http://dx.doi.org/10.1364/AO.49.000196>.

- [47] Pietropoli Charmet A, Tasinato N, Stoppa P, Baldacci A, Giorgianni S. Jet-cooled diode laser spectrum and FTIR integrated band intensities of CF<sub>3</sub>Br: rovibrational analysis of 2ν<sub>5</sub> and ν<sub>2</sub> + ν<sub>3</sub> bands near 9 μm and cross-section measurements in the 450–2500 cm<sup>-1</sup> region. *Mol Phys* 2008;106:1171–9. <http://dx.doi.org/10.1080/00268970802026709>.
- [48] Tasinato N, Pietropoli Charmet A, Stoppa P, Giorgianni S, Buffa G. Spectroscopic measurements of SO<sub>2</sub> line parameters in the 9.2 μm atmospheric region and theoretical determination of self-broadening coefficients. *J Chem Phys* 2010;132:044315. <http://dx.doi.org/10.1063/1.3299274>.
- [49] Orkin VL, Guschin AG, Larin IK, Huie RE, Kurylo MJ. Measurements of the infrared absorption cross-sections of haloalkanes and their use in a simplified calculational approach for estimating direct global warming potentials. *J Photochem Photobiol A* 2003;157(2):211–22. [http://dx.doi.org/10.1016/S1010-6030\(03\)00057-1](http://dx.doi.org/10.1016/S1010-6030(03)00057-1), URL <https://www.sciencedirect.com/science/article/pii/S1010603003000571>. Atmospheric Photochemistry.
- [50] Gordon IE, Rothman LS, Hargreaves RJ, Hashemi R, Karlovets EV, Skinner FM, Conway EK, Hill C, Kochanov RV, Tan Y, Wcislo P, Finenko AA, Nelson K, Bernath PF, Birk M, Boudon V, Campargue A, Chance KV, Coustenis A, Drouin BJ, Flaud JM, Gamache RR, Hodges JT, Jacquemart D, Mlawer EJ, Nikitin AV, Perevalov VI, Rotger M, Tennyson J, Toon GC, Tran H, Tyuterev VG, Adkins EM, Baker A, Barbe A, Canè E, Császár AG, Dudaryonok A, Egorov O, Fleisher AJ, Fleurbaey H, Foltynowicz A, Furtenbacher T, Harrison JJ, Hartmann J-M, Horneman VM, Huang X, Karman T, Karns J, Kass S, Kleiner I, Kofman V, Kwabia-Tchana F, Lavrentieva NN, Lee TJ, Long DA, Lukeševskaya AA, Lyulin OM, Makhnev VY, Matt W, Massie ST, Melosso M, Mikhailenko SN, Mondelain D, Müller HSP, Naumenko OV, Perrin A, Polyansky OL, Raddaoui E, Raston PL, Reed ZD, Rey M, Richard C, Tóbiás R, Sadiek I, Schwenke DW, Starikova E, Sung K, Tamassia F, Tashkun SA, Vander Auwera J, Vasilenko IA, Viganin AA, Villanueva GL, Vispoel B, Wagner G, Yachmenev A, Yurchenko SN. The HITRAN2020 molecular spectroscopic database. *J Quant Spectrosc Radiat Transfer* 2022;277:107949. <http://dx.doi.org/10.1016/j.jqsrt.2021.107949>.
- [51] Sharpe SW, Johnson TJ, Sams RL, Chu PM, Rhoderick GC, Johnson PA. Gas-phase databases for quantitative infrared spectroscopy. *Appl Spectrosc* 2004;58(12):1452–61. <http://dx.doi.org/10.1366/000370204264128>.
- [52] Sihra K, Hurley MD, Shine KP, Wallington TJ. Updated radiative forcing estimates of 65 halocarbons and nonmethane hydrocarbons. *J Geophys Res Atmos* 2001;106(D17):20493–505. <http://dx.doi.org/10.1029/2000JD900716>.
- [53] Carnimeo I, Puzzarini C, Tasinato N, Stoppa P, Pietropoli Charmet A, Biczysko M, Cappelli C, Barone V. Anharmonic theoretical simulations of infrared spectra of halogenated organic compounds. *J Chem Phys* 2013;139:074310. <http://dx.doi.org/10.1063/1.4817401>.
- [54] Tasinato N, Regini G, Stoppa P, Pietropoli Charmet A, Gambi A. Anharmonic force field and vibrational dynamics of CH<sub>2</sub>F<sub>2</sub> up to 5000 cm<sup>-1</sup> studied by Fourier transform infrared spectroscopy and state-of-the-art ab initio calculations. *J Chem Phys* 2012;136:214302. <http://dx.doi.org/10.1063/1.4720502>.
- [55] Boussefi R, Ceselin G, Tasinato N, Barone V. DFT meets the segmented polarization consistent basis sets: Performances in the computation of molecular structures, rotational and vibrational spectroscopic properties. *J Mol Struct* 2020;1208:127886. <http://dx.doi.org/10.1016/j.molstruc.2020.127886>.
- [56] Bravo I, Aranda A, Hurley MD, Marston G, Nutt DR, Shine KP, Smith K, Wallington TJ. Infrared absorption spectra, radiative efficiencies, and global warming potentials of perfluorocarbons: Comparison between experiment and theory. *J Geophys Res Atmos* 2010;115:D24317. <http://dx.doi.org/10.1029/2010JD014771>.
- [57] Becke AD. Density-functional thermochemistry. III. The role of exact exchange. *J Chem Phys* 1993;98(7):5648–52. <http://dx.doi.org/10.1063/1.464913>.
- [58] Francel MM, Pietro WJ, Hehre WJ, Binkley JS, Gordon MS, DeFrees DJ, Pople JA. Self-consistent molecular orbital methods. XXIII. A polarization-type basis set for second-row elements. *J Chem Phys* 1982;77(7):3654–65. <http://dx.doi.org/10.1063/1.444267>.
- [59] Shine KP, Myhre G. The spectral nature of stratospheric temperature adjustment and its application to halocarbon radiative forcing. *J Adv Model Earth Syst* 2020;12. <http://dx.doi.org/10.1029/2019MS001951>, e2019MS001951.
- [60] Pinnock S, Hurley MD, Shine KP, Wallington TJ, Smyth TJ. Radiative forcing of climate by hydrochlorofluorocarbons and hydrofluorocarbons. *J Geophys Res: Atmos* 1995;100:23227–38. <http://dx.doi.org/10.1029/95JD02323>.
- [61] Hodnebrog Ø, Etminan M, Fuglestvedt JS, Marston G, Myhre G, Nielsen CJ, Shine KP, Wallington TJ. Global warming potentials and radiative efficiencies of halocarbons and related compounds: A comprehensive review. *Rev Geophys* 2013;51:300–78. <http://dx.doi.org/10.1002/rog.20013>.